

Communication

# Original Synthesis of a Nucleolipid for Preparation of Vesicular Spherical Nucleic Acids

Erik Dimitrov<sup>1</sup>, Natalia Toncheva-Moncheva<sup>1,\*</sup> , Pavel Bakardzhiev<sup>1</sup>, Aleksander Forsys<sup>2</sup> , Jordan Doumanov<sup>3</sup>, Kirilka Mladenova<sup>3</sup>, Svetla Petrova<sup>3</sup>, Barbara Trzebicka<sup>2</sup>  and Stanislav Rangelov<sup>1,\*</sup><sup>1</sup> Institute of Polymers, Bulgarian Academy of Sciences, Akad. G. Bonchev St. 103A, 1113 Sofia, Bulgaria<sup>2</sup> Centre of Polymer and Carbon Materials, Polish Academy of Sciences, M. Curie-Sklodowskiej 34, 41-819 Zabrze, Poland<sup>3</sup> Department of Biochemistry, Faculty of Biology, Sofia University St. Kliment Ohridski, Dragan Tsankov Blvd. 8, 1164 Sofia, Bulgaria

\* Correspondence: ntoncheva@polymer.bas.bg (N.T.-M.); rangelov@polymer.bas.bg (S.R.)

**Abstract:** Spherical nucleic acids (SNAs)—nanostructures, consisting of a nanoparticle core densely functionalized with a shell of short oligonucleotide strands—are a rapidly emerging class of nanoparticle-based therapeutics with unique properties and specific applications as drug and nucleic acid delivery and gene regulation materials. In this contribution, we report on the preparation of hollow SNA nanoconstructs by co-assembly of an originally synthesized nucleolipid—a hybrid biomacromolecule, composed of a lipidic residue, covalently linked to a DNA oligonucleotide strand—with other lipids. The nucleolipid was synthesized via a *click* chemistry approach employing initiator-free, UV light-induced thiol-ene coupling of appropriately functionalized intermediates, performed in mild conditions using a custom-made UV light-emitting device. The SNA nanoconstructs were of a vesicular structure consisting of a self-closed bilayer membrane in which the nucleolipid was intercalated via its lipid-mimetic residue. They were in the lower nanometer size range, moderately negatively charged, and were found to carry thousands of oligonucleotide strands per particle, corresponding to a grafting density comparable to that of other SNA structures. The surface density of the strands on the bilayer implied that they adopted an unextended conformation. We demonstrated that preformed vesicular structures could be successfully loaded with either hydrophilic or hydrophobic dyes.

**Keywords:** Spherical nucleic acids; vesicles; liposomes; nucleolipids; oligonucleotides; thiol-ene *click* reaction; light scattering; Cryo-TEM



**Citation:** Dimitrov, E.; Toncheva-Moncheva, N.; Bakardzhiev, P.; Forsys, A.; Doumanov, J.; Mladenova, K.; Petrova, S.; Trzebicka, B.; Rangelov, S. Original Synthesis of a Nucleolipid for Preparation of Vesicular Spherical Nucleic Acids. *Nanomaterials* **2022**, *12*, 3645. <https://doi.org/10.3390/nano12203645>

Academic Editor: Maria Letizia Manca

Received: 19 September 2022

Accepted: 13 October 2022

Published: 18 October 2022

**Publisher's Note:** MDPI stays neutral with regard to jurisdictional claims in published maps and institutional affiliations.



**Copyright:** © 2022 by the authors. Licensee MDPI, Basel, Switzerland. This article is an open access article distributed under the terms and conditions of the Creative Commons Attribution (CC BY) license (<https://creativecommons.org/licenses/by/4.0/>).

## 1. Introduction

Spherical nucleic acids (SNAs) are fascinating 3D nanostructures consisting of a nanoparticle core and an oligonucleotide shell [1–5]. These polyvalent architectures, which can be tuned through the type, number, and orientation of the oligonucleotide strands in the shell and through a broad range of inorganic and organic cores, have quickly gained an important role in nucleic acid-containing formulations [6–8]. They exhibit properties that are distinctly different from those of their constituent counterparts: SNA structures can penetrate the membranes of the cells without using transfection agents, avoid many biological barriers as well as the attack by the human immune system, and deliver the cargo. They exhibit extraordinary stability in physiological environments and resistance to nuclease degradation [9,10]. This makes them effective as high-sensitivity detection systems, and also, ideal for intracellular diagnostic and therapeutic agents [11–15].

To successfully shuttle nucleic acids, loaded drugs, and/or diagnostic agents into cells, SNAs can be properly designed in terms of architecture, functionality, molar mass, size, hydrophilic/lipophilic balance, etc., [16–18]. For instance, the selection of the right nanoparticle core plays a key role and directly determines the shape, size, and biological profiles of the core-shell assemblies [19–21]. Strategies to design SNAs with organic cores,

formed by polymers, lipids, small molecules, and proteins, have recently been developed to obtain biocompatible and biodegradable SNAs [22–25]. Among them, the liposomal SNAs, with their hollow interior and bilayer structural organization emerged as a new class of nucleic acids. They are synthesized by anchoring/intercalation of hydrophobically modified oligonucleotide strands via their hydrophobic residue into the bilayer membrane of phospholipid liposomes [23,26,27]. The advances in the understanding of liposomal SNA constructs reveal that they offer superior antitumor efficacy, higher downstream cellular activity, increased cellular uptake, faster DNA release, and higher DNA-loading capacity over the prototypical SNAs [26,28].

The liposomal SNAs define a new class of SNAs that is held together via non-covalent bonds. They are typically made from phospholipids and cholesterol (both components of the cell membranes) and a small quantity of nucleolipid. Whereas the former two are part of FDA-approved pharmaceuticals, the latter can be specially designed to serve an integral role in the function and behavior of the liposomal SNAs. However, the barrier to the therapeutic use of new materials is high, particularly for such that may have problems with clearance or unknown biodistribution. In this regard, utilization of synthetic routes to circumvent any possible contaminations in the resulting nucleolipids, which can pose a considerable challenge in their efficient removal, is of significant importance. The *click* chemistry approaches offer such a possibility. These coupling reactions are straightforward and typically proceed in mild conditions, give quantitative yields, and allow simple isolation of products. The strategy is based on separate preparations of “clickable” entities (here, an oligonucleotide strand and a lipophilic moiety) and their coupling into a novel architecture. Importantly, it makes it possible to achieve combinations of species that are inaccessible by conventional methods, e.g., phosphoramidite chemistry for the synthesis of nucleolipids. Among the various *click* reactions, the most generally used ones require metal catalysts or radical initiators, which may pose some drawbacks associated with the use of, e.g., Cu(I) in biological systems [29] or DNA degradation [30]. Herein, we employ an original synthetic approach for the preparation of a nucleolipid by covalently joining a lipid-mimetic double chain residue with a 21-base-long nucleic acid strand using initiator-free, UV light-induced thiol-ene *click* reaction. Further, by simple intercalation of the novel nucleolipid in the phospholipid bilayer of liposomes, well-defined liposomal SNA structures are obtained and fully characterized. The loading capability of the structures with respect to hydrophilic and hydrophobic substances is examined as well.

## 2. Materials and Methods

1-Hexadecanol, hexadecyl glycidyl ether, allyl glycidyl ether, SnCl<sub>4</sub>, potassium (cubes in mineral oil), 2-aminoethanethiol hydrochloride, poly(ethylene glycol) methyl ether thiol (PEGMET, M<sub>w</sub> = 2000 g/mol), 1,2-dipalmitoyl-rac-glycero-3-phosphocholine (DPPC), and cholesterol (Chol), all products of Sigma-Aldrich, were used as received. Hexane (Sigma-Aldrich, Saint Louis, MO, USA), 1,4-dioxane (Sigma-Aldrich), methylene chloride (Fisher Scientific, Waltham, MA, USA), toluene (Fisher Scientific), benzene (Merck, Darmstadt, Germany), methanol (Sigma-Aldrich), and tetrahydrofuran (Fisher Scientific) were dried with calcium hydride and freshly distilled before use. N,N-Dimethylformamide (DMF, ACS reagent, ≥99.8%) and dimethyl sulfoxide (DMSO, ACS reagent, ≥99.9%) were dried by molecular sieves. Deionized water was obtained by a Millipore MilliQ system and was additionally filtered through a 220 nm PTFE filter and a 20 nm cellulose filter. Thiol-functionalized oligonucleotide (ThiolC<sub>6</sub>-oligonucleotide) was purchased from Biomers.net GmbH. The sequence and composition as well as characterization data, according to the producer, are presented in Table S1 and Figure S1 of Supplementary Materials. Details for the synthesis and characterization of dihexadecyloxy-propane-2-ol (DHP) and spacer-modified DHP-(AGE)<sub>n</sub> are given in Supplementary Materials (Figures S2–S4).

*Synthesis of the nucleolipid DHP-(AGE)<sub>3</sub>-oligonucleotide.* A total of 491.3 μg (61.4 nmol, 1 eq.) of thiolated oligonucleotide, and 197.4 μg (223 nmol, 3.6 eq.) of DHP-(AGE)<sub>3</sub> were dissolved in a 2.5 mL solvent mixture of DMF:DMSO:H<sub>2</sub>O (*v/v* 0.45:0.45:0.1) and placed in a

round-bottom flask under vigorous stirring, flushed with argon, and wrapped in aluminum foil. The UV light-induced thiol-ene *click* reaction was carried out for 1 h at 30 °C and the full (4 W) capacity of the UV irradiation device. Detailed information for the device is given in the Supplementary Materials (Figure S5). The reaction mixture was cooled to room temperature and purified by intense dialysis against a mixture of DMSO:DMF (*v/v* 1:1) for 2 days using an 8 kDa MWCO membrane. Then the organic dialysis solvent was replaced with ultra-pure MilliQ water followed by ultrafiltration for additional 3 days yielding a clear to slightly opalescent aqueous dispersion of the nucleolipid DHP-(AGE)<sub>3</sub>-oligonucleotide. Finally, the sample was freeze dried. Yield: 470 µg, 85%.

*Preparation of vesicular SNAs.* Stock solutions of known concentrations of DPPC and Chol in chloroform and the nucleolipid DHP-(AGE)<sub>3</sub>-oligonucleotide in methanol were prepared. Predefined amounts of these solutions were placed into glass tubes to achieve 2 mM total lipid concentration, 2:1 DPPC:Chol M ratio, and 2 mol % of nucleolipid as follows: 0.04 µmol (301.90 µg) of nucleolipid, 1.30 µmol (954.2 µg) of DPPC, and 0.65 µmol (251.55 µg) of Chol. The solvent ratio was kept in the 1:9–1:10 range with respect to methanol in order to avoid precipitation. After mixing, the solvents were removed under a gentle stream of argon leaving a thin film. All traces of solvent were removed under a vacuum overnight at room temperature. The dry, thin lipid film was hydrated with 1 mL of MilliQ water and the resulting dispersion was subjected to ten freeze–thaw cycles and then extruded 15 times through polycarbonate filters (100 nm pore size) using a handle-type extruder (Avanti Polar Lipids, Alabaster, AL, USA).

*Nuclear Magnetic Resonance (<sup>1</sup>H-NMR).* <sup>1</sup>H-NMR measurements were conducted on a Bruker Avance II spectrometer operating at 600 MHz using CDCl<sub>3</sub>, DMSO-d<sub>6</sub>, or benzene-d<sub>6</sub> at 25 °C.

*Size Exclusion Chromatography (SEC).* SEC analyses were performed on a Shimadzu Nexera HPLC chromatograph equipped with a degasser, a pump, an autosampler, an RI detector, and three columns: 10 µm PL gel mixed-B and 5 µm PL gel 500 Å and 50 Å. Tetrahydrofuran was used as the eluent at a flow rate of 1.0 mL·min<sup>−1</sup> and temperature of 40 °C. The sample concentration was 1 mg·mL<sup>−1</sup>, and SEC was calibrated with polystyrene standards.

*Light Scattering.* Dynamic light scattering (DLS) measurements were performed on a Brookhaven BI-200 goniometer with vertically polarized incident light at a wavelength λ = 633 nm supplied by a He–Ne laser operating at 35 mW and equipped with a Brookhaven BI-9000 AT digital autocorrelator. Measurements were made at an angle of 90° and 37 °C. The autocorrelation functions were analyzed using the constrained regularized algorithm CONTIN [31] to obtain the distributions of the relaxation rates (Γ<sub>90</sub>). The latter provided distributions of the apparent diffusion coefficient (D<sub>90</sub> = Γ<sub>90</sub>/q<sup>2</sup>) where q is the magnitude of the scattering vector given by q = (4πn/λ)sin(θ/2), n is the refractive index of the medium, and θ = 90°. The mean hydrodynamic radius was obtained by the Stokes–Einstein equation (Equation (1)):

$$R_h = kT / (6\pi\eta D_{90}) \quad (1)$$

where k is the Boltzmann constant, and η is the solvent viscosity at temperature T in Kelvin.

*Electrophoretic Light Scattering:* The electrophoretic light scattering measurements were carried out on a 90Plus PALS instrument (Brookhaven Instruments Corporation, Hostville, NY, USA), equipped with a 35 mW red diode laser (λ = 640 nm) at a scattering angle (θ) of 15°. ζ potentials were calculated from the obtained electrophoretic mobility at 37 °C by using the Smoluchowski Equation (2):

$$\zeta = 4\pi\eta v / \epsilon \quad (2)$$

where η is the solvent viscosity, v is the electrophoretic mobility, and ε is the dielectric constant of the solvent.

*Cryogenic Transmission Electron Microscopy (Cryo-TEM).* Cryo-TEM images were obtained using a Tecnai F20 X TWIN microscope (FEI Company, Hillsboro, OR, USA) equipped

with a field-emission gun, operating at an acceleration voltage of 200 kV. Images were recorded on the Gatan Rio 16 CMOS 4k camera an Eagle 4k HS camera (Gatan Inc., Pleasanton, CA, USA) and processed with Gatan Microscopy Suite (GMS) software (Gatan Inc., Pleasanton, CA, USA). Specimen preparation was done by the vitrification of the aqueous dispersions on grids with a holey carbon film (Quantifoil R 2/2; Quantifoil Micro Tools GmbH, Großlobichau, Germany). Prior to use, the grids were activated for 15 s in oxygen plasma using a Femto plasma cleaner (Diener Electronic, Ebhausen, Germany). Cryo-samples were prepared by applying a droplet (3  $\mu$ L) of the dispersion to the grid, blotting with filter paper and immediate freezing in liquid ethane using a fully automated blotting device Vitrobot Mark IV (Thermo Fisher Scientific, Waltham, MA, USA). After preparation, the vitrified specimens were kept under liquid nitrogen until they were inserted into a cryo-TEM holder Gatan 626 (Gatan Inc., Pleasanton, CA, USA) and analyzed at  $-178$  °C.

**Gel electrophoresis.** The completeness of the *click* coupling reaction was confirmed by agarose gel electrophoresis. Gels containing 1% agarose (*w/w*) were run on an FBSB-710 electrophoresis unit (Fisher Biotech) in  $1 \times$  Tris-Borate EDTA (TBE) buffer at room temperature and 50 V. Imaging was carried out by ethidium bromide staining and UV illumination (302 nm). Quick-Load<sup>®</sup> Purple 1 kb DNA Ladder of BioLabs was used as a marker. Total amounts of 0.6  $\mu$ g were loaded. The gels were imaged using a gel reader Alpha Innotech.

**Fluorescence microscopy.** The vesicular SNAs were incubated with Laurdan (Sigma Aldrich) in a final concentration of 25  $\mu$ M Laurdan in DMSO for 30 min at 37 °C [32]. For the covalent binding of fluorescein isothiocyanate (FITC, final concentration 5 mM) (Sigma Aldrich) to vesicular SNAs, incubation was performed for 2 h at room temperature [33]. After incubation, vesicular SNAs were dialyzed against phosphate buffer pH 7.4 for 2 h at room temperature. Vesicular SNAs were visualized with a fluorescence microscope (GE Delta Vision Ultra Microscopy System) with a 60 $\times$  immersion objective.

### 3. Results and Discussion

#### 3.1. Synthesis and Characterization of the Nucleolipid

We designed a novel nucleolipid, comprising a lipid-mimetic residue covalently attached to a short (21 bases long) single-stranded DNA oligonucleotide. The synthesis was realized by an initiator-free, UV-induced thiol-ene *click* reaction using a custom-made irradiation device (see Supplementary Materials for the description of the device). The synthetic route for the preparation of the nucleolipid is shown in Figure 1. Briefly, the lipid-mimetic anchor, 1,3-dihexadecyloxy-propane-2-ol (DHP), prepared as described elsewhere [34,35], was modified by introducing a short spacer with an average of three allyl glycidyl ether units, (AGE)<sub>3</sub>. The introduction of a spacer has been shown critical for further modification of the secondary hydroxyl group of DHP [27]. Furthermore, the spacer segment pushes the oligonucleotide strand away from the lipid-mimetic anchor, which gives more freedom to the former for various interactions. We selected a polyether spacer, which, in contrast to other common polyether spacers such as poly(ethylene glycol) or poly(propylene glycol), is not chemically inert: it contains allyl functionality, which can be exploited for various orthogonal modifications including radical addition of thiols. The target degree of polymerization was just a few units because poly(allyl glycidyl ether) is a hydrophobic polymer [36] and longer chains would introduce significant hydrophobicity in the final nucleolipid. The formation of the spacer was achieved by anionic ring-opening polymerization of AGE initiated by partially deprotonated DHP, thus, forming DHP-(AGE)<sub>n</sub> intermediate (Figure 1a). The SEC analysis showed a monomodal molar mass distribution ( $M_w^{SEC} = 1350$  g.mol<sup>-1</sup>,  $M_w/M_n = 1.1$ , see Figure S4), which is typical for the polymerization technique used. Since the molar mass from SEC is relative to polystyrene standards, the average degree of polymerization of the (AGE)<sub>n</sub> spacer was determined from the <sup>1</sup>H NMR spectrum of the product shown in Figure 2a. The average number of AGE units ( $n = 3$ ) was calculated from the integral ratio of the signal for the methyl protons (protons *a* at 0.85 ppm) to methine protons of the allyl groups (protons *i* at 5.80 ppm).

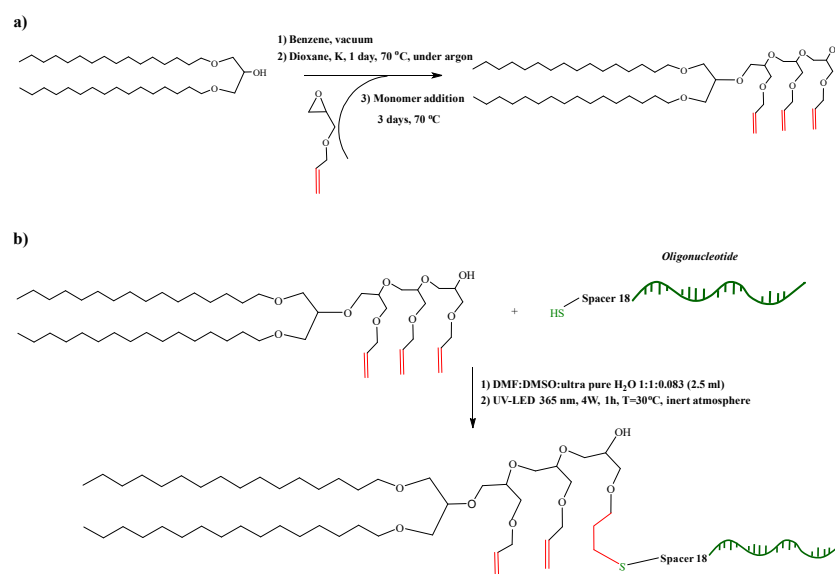


**Figure 1.** Synthetic schemes for preparation of (a) the DHP-(AGE)<sub>n</sub> intermediate (n = 3) and (b) the nucleolipid DHP-(AGE)<sub>3</sub>-oligonucleotide.

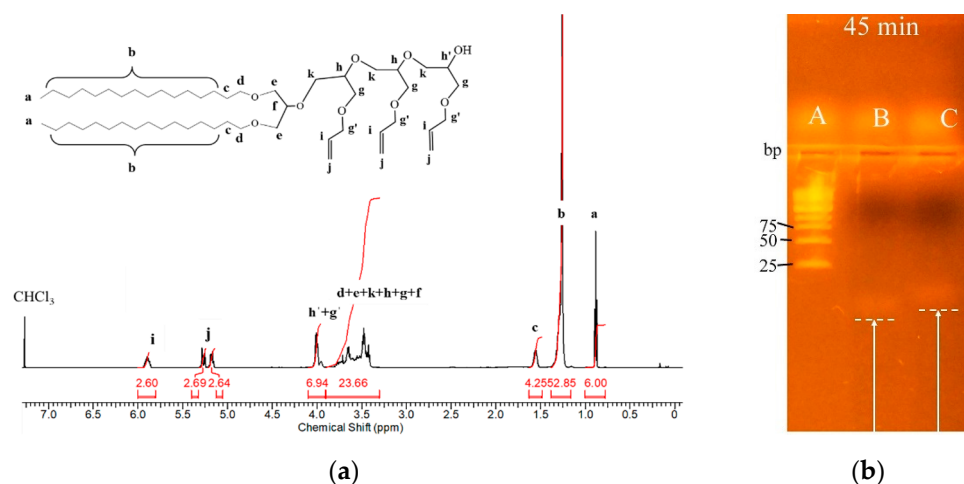


**Figure 2.** (a) <sup>1</sup>H NMR spectrum of the intermediate DHP-(AGE)<sub>n</sub> (n = 3) in CDCl<sub>3</sub>. (b) Agarose gel retardation patterns of thiolated oligonucleotide and the nucleolipid DHP-(AGE)<sub>3</sub>-oligonucleotide. The white arrows indicate the different retardations of the thiolated oligonucleotide (lane B) and nucleolipid (lane C). Nucleic acids were stained with ethidium bromide. Overall duration of the experiment 45 min as indicated. Lane A: molecular weight marker.

The conjugation of the oligonucleotide to DHP-(AGE)<sub>3</sub> was performed via the thiol-ene coupling reaction. The reaction is orthogonal [37], tolerant to a variety of functional groups and can be performed in aqueous media. Normally, the thiol-ene coupling reaction can be initiated by UV light, which induces the formation of a thiol radical that reacts with the carbon–carbon double bond to produce a thioether. In that aspect, the (AGE)<sub>n</sub> spacer offers another benefit: since each unit of the spacer carries a double bond, the number of sites on which the coupling reaction takes place is increased. As UV light and free radicals can be harmful to nucleic acids, we performed model reactions to find optimal conditions for the thiol-ene coupling reaction (see Supplementary Materials, Figure S6). Firstly, we determined that the safe UV irradiation time for the oligonucleotides is 1 h at 30 °C, λ = 365 nm, and the full capacity (4 W) of the device. Next, model reactions of DHP-(AGE)<sub>n</sub> with 2-aminoethanethiol hydrochloride and poly(ethylene glycol) methyl ether thiol (PEGMET, M<sub>w</sub> = 2000 g/mol), representing low- and high molar mass thiolated compounds, respectively, were performed (see Supplementary Materials). The results

revealed that 2-aminoethanthal hydrochloride reacted with two, whereas PEGMET with only one, presumably the outermost, of the double bonds of the  $(AGE)_n$  spacer (see Supplementary Materials, Figures S7–S10).

The coupling reaction between DHP- $(AGE)_n$  and thiolated oligonucleotide was performed at the above conditions in a large excess of DHP- $(AGE)_n$  in a mixed DMSO/DMF/water solvent (Figure 1b). After the reaction was accomplished, the system was cooled down to room temperature and subjected to dialysis against DMF:DMSO to remove the excess of DHP- $(AGE)_n$ . Afterwards, the mixed solvent was displaced by ultrafiltration, which yielded a dilute aqueous dispersion of the resulting nucleolipid. The latter was characterized by gel electrophoresis (Figure 2b). Ethidium bromide was used for visualizing and identifying the nucleic acid bands. It has been shown to bind to single-stranded nucleic acids although less strongly than to double-stranded ones [38]. Therefore, the fluorescence was lower and the bands of the oligonucleotide and nucleolipid were weaker compared to those of the molecular weight marker. Nevertheless, the retardation of the electrophoretic mobility of the nucleolipid compared to that of the thiolated oligonucleotide, used as control, is clearly visible in Figure 2b and is consistent with the enlargement of the molecular weight of the nucleolipid.

### 3.2. Preparation of Vesicular SNAs

Vesicular SNAs have been synthesized by surface functionalization of pre-formed phospholipid liposomes with DNA strands modified with a hydrophobic tail [26] and by co-assembly of a phospholipid (1,2-dipalmitoyl-rac-glycero-3-phosphocholine, DPPC) and an original nucleolipid composed of a lipid-mimetic residue covalently attached to a DNA oligonucleotide strand [27]. Following a common route for the preparation of small unilamellar vesicles involving thin film hydration, freeze-thawing of the dispersions, and multiple extrusion through small pore size filters, we prepared vesicular structures consisting of a self-closed oligonucleotide-grafted bilayer membrane (Figure 3). In a parallel experiment plain DPPC/Chol liposomes were prepared following the same preparation procedure.

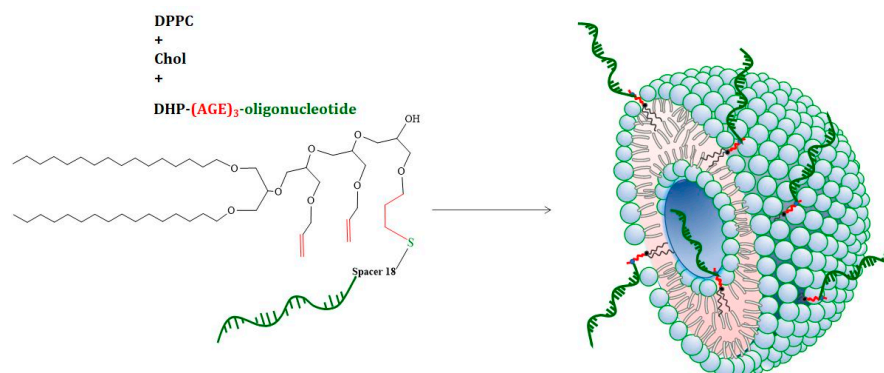


**Figure 3.** Schematics of the formation of vesicular SNAs from DPPC, cholesterol, and nucleolipid.

The successful incorporation of the nucleolipid was evidenced by the appearance of absorption at 260 nm, which is characteristic of nucleic acids [39], in the UV-Vis spectrum of the purified dispersion (Figure 4a). Dynamic and electrophoretic light scattering measurements further evidenced the formation of vesicular SNAs. Compared to the plain DPPC/Chol liposomes, the vesicular SNAs were smaller in size and more negatively charged (Figure 4b and Table 1). Whereas the latter can be anticipated, the size decrease upon the incorporation of the nucleolipid in the bilayer might seem somewhat counterintuitive but can be rationalized in terms of repulsive interactions between the oligonucleotide strands that create curving of the bilayer. More curved bilayers (that is, vesicles of a smaller size) would give bigger relaxation of the repulsive interactions [40]. The particles were visualized by cryo-TEM (Figure 4c). Clearly, all objects were unilamellar vesicles of spherical morphology and dimensions that were compatible with the size determined by dynamic

light scattering. The bilayer membranes were intact with a constant thickness of about 5 nm, which is consistent with DPPC systems [41]. Changes in the characterization parameters of the vesicular SNAs were not detected for ca. two months, which implied enhanced colloidal stability.

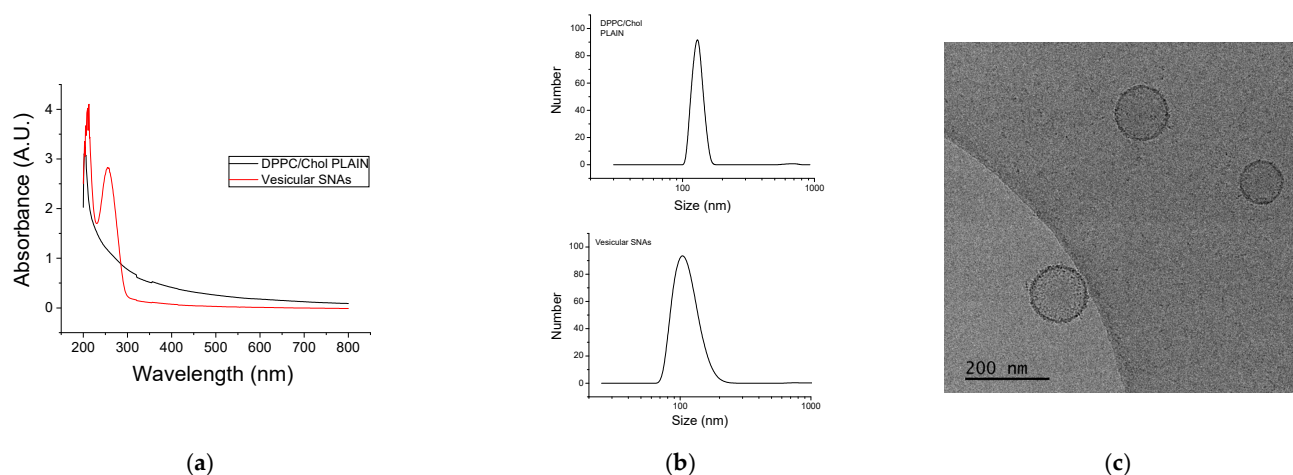


**Figure 4.** (a) UV-Vis spectra of vesicular SNAs and plain DPPC/Chol liposomes. (b) Size distributions from DLS of plain DPPC/Chol liposomes and vesicular SNAs as indicated. (c) Cryo-TEM images of vesicular SNAs.

**Table 1.** Light scattering parameters and other characterization data of plain DPPC/Chol liposomes and vesicular SNAs, prepared by co-assembly of DPPC, cholesterol, and nucleolipid. Measurements were performed at 37 °C.

	$R_h^*$ (nm)	$\zeta$ Potential (mV)	Number of Strands per Vesicle	Surface Coverage	
				( $\text{nm}^{-2}$ )	$\text{pmol}\cdot\text{cm}^{-2}$
Plain DPPC/Chol liposomes	$67.4 \pm 3.4$ (0.087)	$-0.34 \pm 0.01$	n.a.	n.a.	n.a.
Vesicular SNAs	$57.1 \pm 2.9$ (0.127)	$-9.11 \pm 0.36$	$3880 \pm 194$	0.047	7.8

\* PDI values in parentheses.

The synthesized vesicular SNAs had an average number of  $3880 \pm 194$  strands per particle (Table 1) as calculated from the feed/stoichiometry (DPPC and oligonucleotide contents) and size of the vesicles (see Supplementary Materials). The value is larger than that of reference samples (micellar and liposomal SNAs, gold nanoparticles SNAs) [22,42–46] but is consistent with the relatively larger size of the present vesicular structures. The surface coverage,  $\sigma$ , expressed as number of strands per squared nm,  $\sigma = 0.047 \text{ nm}^{-2}$ , and converted into amount of nucleolipid per squared cm,  $\sigma = 7.8 \text{ pmol}\cdot\text{cm}^{-2}$  (Table 1, see Supplementary Materials), was of the same magnitude to those obtained for previously reported SNA structures [17,22,42–46] as well as oligonucleotides immobilized on solid substrates [47] considering that  $\sigma$  is dependent on particle size and shape [1] and can be controlled by the salt [48] and nucleolipid contents.

The conformation of the oligonucleotide strands can be estimated by comparing the values of the grafting density with the critical grafting density ( $\sigma_{\text{cr}}$ ) at the transition to strongly extended, brush conformation. Regarding the oligonucleotide strands as surface-anchored random coils, the transition from the unextended to the brush conformation, which defines two concentration regimes [49,50], can be determined by  $\sigma_{\text{cr}} = 1/R_F^2$  where  $R_F$  is the Flory radius (see Supplementary Materials for the calculation of  $R_F$  and  $\sigma_{\text{cr}}$ ). Since for the investigated system  $\sigma (=0.047 \text{ nm}^{-2})$  is smaller than  $\sigma_{\text{cr}} (=0.156 \text{ nm}^{-2})$ , one may

conclude that the oligonucleotide strands adopt an unextended conformation and hardly interact laterally. However, as discussed elsewhere [17], none of the SNA constructs hitherto reported exhibit grafting density values larger than  $\sigma_{cr}$ , indicating that the oligonucleotide strands have not entered the brush regime. Notwithstanding, these structures have been shown to manifest the typical SNA properties [26].

The vesicular SNAs were loaded with model compounds that exhibit diametrically opposite solubility and different properties. Fluorescein isothiocyanate (FITC), which has the potential for covalent binding with DNA [33], and laurdan—used to investigate membrane quality of phospholipid bilayers [51]—were selected as hydrophilic and lipophilic, respectively, probes. Preformed vesicular SNAs were incubated with the two dyes and, after removing the unloaded material by dialysis, were analyzed by dynamic and electrophoretic light scattering and visualized by fluorescence microscopy (Figure 5). Noteworthy, their size and  $\zeta$  potential practically did not change upon loading—the values of the hydrodynamic radius and  $\zeta$  potential were within the standard deviations (see Table 1). Since the vesicles were not sufficiently large (the resolution of conventional fluorescence microscopy is limited by diffraction to about 200 nm in the focal plane and to about 500 nm along the optic axis), the method provided only qualitative evidence for successful loading. The images showed bright, about micron-size, mostly spherical objects. The sizes were larger than what was observed by dynamic light scattering (see above) which can be attributed to the clustering of SNAs during the preparation step for observation. The findings revealed the potential of the vesicular SNAs to incorporate both hydrophilic and hydrophobic compounds individually and, most probably, simultaneously, in accordance with their specific structure.

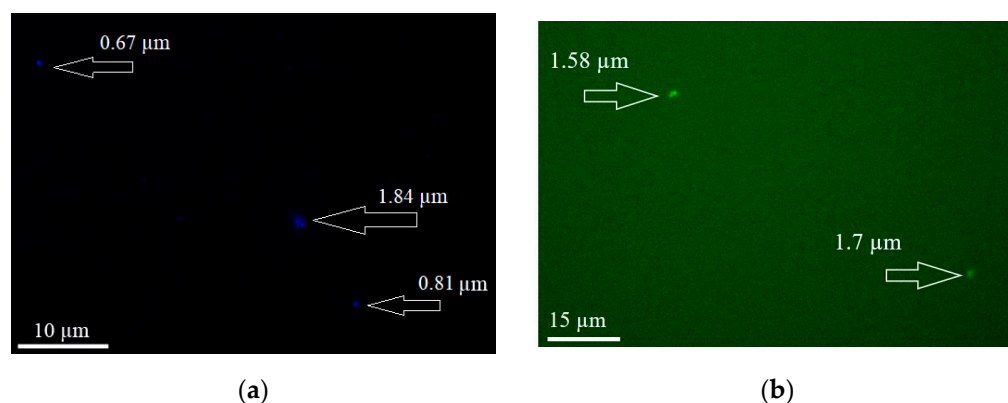


**Figure 5.** Fluorescent labeling of vesicular SNAs with (a) laurdan and (b) FITC.

#### 4. Conclusions

A novel nucleolipid consisting of a lipid-mimetic double-chain residue covalently attached to a single-stranded DNA oligonucleotide was synthesized by an initiator-free, UV-induced thiol-ene *click* reaction. The reaction was performed in mild conditions using a custom-made UV irradiation device. Optimal synthetic parameters of the reaction in terms of reaction conditions, on one hand, and safety (with regard to oligonucleotides), effectiveness, and yield, on the other, were established. The introduction of a spacer bearing multiple allyl functionalities to increase the reaction sites on which the coupling reaction takes place, was of significant importance to effectively perform the coupling reaction and obtain the product in good yield. The reaction is applicable to thiolated oligonucleotides independently of the type (DNA or RNA) and sequence. Unilamellar vesicles consisting of a self-closed oligonucleotide-grafted bilayer membrane were successfully prepared by co-assembly of the nucleolipid with readily available lipids DPPC and cholesterol. The vesicles were found to carry thousands ( $3880 \pm 194$ ) of oligonucleotide strands per particle, corresponding to grafting density comparable to that of other SNA structures. The value of the grafting density implied that the oligonucleotide strands did not adopt a fully extended conformation. Preformed vesicles were easily and spontaneously loaded

with model compounds exhibiting different solubility properties. Consequently, these structures show promise as carriers for two or more payloads—the nucleic acid component that can be designed with a specific sequence for, e.g., gene silencing, and hydrophilic or hydrophobic drugs separately or together. Such constructs can bypass the need for a co-carrier system in combination therapy and allow one to access simultaneously a gene target and a drug target.

**Supplementary Materials:** The following supporting information can be downloaded at: <https://www.mdpi.com/article/10.3390/nano12203645/s1>, Section I. Composition and characterization of ThiolC<sub>6</sub>-oligonucleotide; Section II. Synthesis of dihexadecyloxy-propane-2-ol (DHP); Section III. Synthesis of DHP-(AGE)<sub>n</sub>; Section IV. Description of the UV irradiation device; Section V. Model reactions (Determination of the safe irradiation time; conjugation of DHP-(AGE)<sub>n</sub> with 2-aminoethanethiol hydrochloride; conjugation of DHP-(AGE)<sub>n</sub> with PEGMET); Section VI. Calculation of the average number of oligonucleotide strands per vesicle and grafting density; Section VII. Calculation of the Flory radius, R<sub>F</sub>, and determination of the critical grafting density ( $\sigma_{cr}$ ) at the transition from mushroom to brush conformation; Figure S1: HPLC chromatogram (left), MALDI spectrum (right), and other characterization data of ThiolC<sub>6</sub>-oligonucleotide; Figure S2: <sup>1</sup>H-NMR spectrum of 1,3-dihexadecyloxy-propane-2-ol in CDCl<sub>3</sub>; Figure S3: Schematic presentation of the synthesis of 1,3-dihexadecyloxy-propane-2-ol; Figure S4: Photograph of the UV irradiation device; Figure S5: UV-Vis spectra of sacrificial oligonucleotides in water (a) and DMF:DMSO (*v/v* 1:1) solvent mixture (b) irradiated by UV light ( $\lambda = 365$  nm, full capacity of 4 W of the device) in inert atmosphere at 30 °C and gentle stirring. Spectra were taken at different time intervals as indicated. Peak maxima at 260 nm and 275 nm in (a) and (b), respectively; Figure S6: <sup>1</sup>H NMR spectra of the DHP-(AGE)<sub>3</sub>/aminoethanethiol hydrochloride reaction mixture. Spectra were taken in DMSO-d<sub>6</sub> at different time intervals as indicated; Figure S7: Schematic presentation of the coupling reaction of DHP-(AGE)<sub>3</sub> with 2-aminoethanethiol hydrochloride; Figure S8: <sup>1</sup>H NMR spectra of DHP-(AGE)<sub>3</sub>/PEGMET reaction mixture. Spectra were taken in deuterated benzene at different time intervals as indicated; Figure S9: Schematic presentation of the coupling reaction of DHP-(AGE)<sub>3</sub> with PEGMET; Table S1: t Sequence and composition of the ThiolC<sub>6</sub>-oligonucleotide. References [34,35,41,52–54] are cited in supplementary materials.

**Author Contributions:** Conceptualization, S.R. and N.T.-M.; Data curation, E.D., P.B., A.F. and K.M.; Formal analysis, E.D., P.B., A.F., K.M. and J.D.; Funding acquisition, S.R., J.D. and N.T.-M.; Investigation, E.D., N.T.-M., P.B., A.F., K.M., S.P., J.D., B.T. and S.R.; Methodology, E.D., A.F., S.P., K.M. and P.B.; Project administration, S.R., N.T.-M. and J.D.; Resources, S.R. and J.D.; Supervision, S.R., B.T., S.P. and J.D.; Validation, E.D., P.B., A.F., K.M. and N.T.-M.; Writing—original draft, N.T.-M. and S.R.; Writing—review and editing, E.D., N.T.-M., P.B., A.F., J.D., K.M., S.P., B.T. and S.R. All authors have read and agreed to the published version of the manuscript.

**Funding:** This research was funded by the National Science Fund (Bulgaria), grant number DN19/8-2017.

**Acknowledgments:** Research equipment of Distributed Research Infrastructure INFRAMAT, part of the Bulgarian National Roadmap for Research Infrastructures, supported by the Bulgarian Ministry of Education and Science, was used in this investigation.

**Conflicts of Interest:** The authors declare no conflict of interest.

## References

1. Cutler, J.I.; Auyeung, E.; Mirkin, C.A. Spherical Nucleic Acids. *J. Am. Chem. Soc.* **2012**, *134*, 1376–1391. [[CrossRef](#)] [[PubMed](#)]
2. Mokhtarzadeh, A.; Vahidnezhad, H.; Youssefian, L.; Mosafer, J.; Baradaran, B.; Uitto, J. Applications of Spherical Nucleic Acid Nanoparticles as Delivery Systems. *Trends Mol. Med.* **2019**, *25*, 1066–1079. [[CrossRef](#)] [[PubMed](#)]
3. Banga, R.J.; Krovi, S.A.; Narayan, S.P.; Sprangers, A.J.; Liu, G.; Mirkin, C.A.; Nguyen, S.T. Drug-loaded Polymeric Spherical Nucleic Acids: Enhancing Colloidal Stability and Cellular Uptake of Polymeric Nanoparticles through DNA Surface-functionalization. *Biomacromolecules* **2017**, *18*, 483–489. [[CrossRef](#)] [[PubMed](#)]
4. Williams, S.C.P. Spherical nucleic acids: A whole new ball game. *Proc. Natl. Acad. Sci. USA* **2013**, *110*, 13231–13233. [[CrossRef](#)] [[PubMed](#)]
5. Song, Y.; Song, W.; Lan, X.; Cai, W.; Jiang, D. Spherical nucleic acids: Organized nucleotide aggregates as versatile nanomedicine. *Aggregate* **2022**, *3*, e120. [[CrossRef](#)] [[PubMed](#)]

6. Zheng, D.; Giljohann, D.A.; Chen, D.L.; Massich, M.D.; Wang, X.-Q.; Iordanov, H.; Mirkin, C.A.; Paller, A.S. Topical delivery of siRNA-based spherical nucleic acid nanoparticle conjugates for gene regulation. *Proc. Natl. Acad. Sci. USA* **2012**, *109*, 11975–11980. [[CrossRef](#)]
7. Briley, W.; Halo, T.L.; Randeria, P.S.; Alhasan, A.H.; Auyeung, E.; Hurst, S.J.; Mirkin, C.A. Biochemistry and Biomedical Applications of Spherical Nucleic Acids (SNAs). In *Nanomaterials for Biomedicine*; Nagarajan, R., Ed.; ACS Symposium Series; American Chemical Society: Washington, DC, USA, 2012; pp. 1–20.
8. Banga, R.J.; Meckes, B.; Narayan, S.P.; Sprangers, A.J.; Nguyen, S.T.; Mirkin, C.A. Cross-Linked Micellar Spherical Nucleic Acids from Thermoresponsive Templates. *J. Am. Chem. Soc.* **2017**, *139*, 4278–4281. [[CrossRef](#)] [[PubMed](#)]
9. Giljohann, D.A.; Seferos, D.S.; Prigodich, A.E.; Patel, P.C.; Mirkin, C.A. Gene regulation with polyvalent siRNA-nanoparticle conjugates. *J. Am. Chem. Soc.* **2009**, *131*, 2072–2073. [[CrossRef](#)] [[PubMed](#)]
10. Seferos, D.S.; Prigodich, A.E.; Giljohann, D.A.; Patel, P.C.; Mirkin, C.A. Polyvalent DNA Nanoparticle Conjugates Stabilize Nucleic Acids. *Nano Lett.* **2009**, *9*, 308–311. [[CrossRef](#)] [[PubMed](#)]
11. Barnaby, S.N.; Sita, T.L.; Petrosko, S.H.; Stegh, A.H.; Mirkin, C.A. Therapeutic applications of spherical nucleic acids. *Cancer Treat. Res.* **2015**, *166*, 23–50. [[CrossRef](#)] [[PubMed](#)]
12. Benizri, S.; Gissot, A.; Martin, A.; Vialet, B.; Grinstaff, M.W.; Barthélémy, P. Bioconjugated Oligonucleotides: Recent Developments and Therapeutic Applications. *Bioconjug. Chem.* **2019**, *30*, 366–383. [[CrossRef](#)] [[PubMed](#)]
13. Kapadia, C.H.; Melamed, J.R.; Day, E.S. Spherical Nucleic Acid Nanoparticles: Therapeutic Potential. *BioDrugs* **2018**, *32*, 297–309. [[CrossRef](#)] [[PubMed](#)]
14. Liu, H.; Kang, R.S.; Bagnowski, K.; Yu, J.M.; Radecki, S.; Daniel, W.L.; Anderson, B.R.; Nallagat, S.; Schook, A.; Agarwal, R.; et al. Targeting the IL-17 Receptor Using Liposomal Spherical Nucleic Acids as Topical Therapy for Psoriasis. *J. Investig. Dermatol.* **2020**, *140*, 435–444. [[CrossRef](#)] [[PubMed](#)]
15. Choi, C.H.; Hao, L.; Narayan, S.P.; Auyeung, E.; Mirkin, C.A. Mechanism for the endocytosis of spherical nucleic acid nanoparticle conjugates. *Proc. Natl. Acad. Sci. USA* **2013**, *110*, 7625–7630. [[CrossRef](#)] [[PubMed](#)]
16. Bakardzhiev, P.; Toncheva-Moncheva, N.; Mladenova, K.; Petrova, S.; Videv, P.; Moskova-Doumanova, V.; Topouzova-Hristova, T.; Doumanov, J.; Rangelov, S. Assembly of amphiphilic nucleic acid-polymer conjugates into complex superaggregates: Preparation, properties, and in vitro performance. *Eur. Polym. J.* **2020**, *131*, 109692. [[CrossRef](#)]
17. Haladjova, E.; Ugrinova, I.; Rangelov, S. One-pot Synthesis of Oligonucleotide-Grafted Polymeric Nanoparticles. *Soft Matter* **2020**, *16*, 191–199. [[CrossRef](#)] [[PubMed](#)]
18. Hong, B.J.; Eryazici, I.; Bleher, R.; Thaner, R.V.; Mirkin, C.A.; Nguyen, S.T. Directed Assembly of Nucleic Acid-Based Polymeric Nanoparticles from Molecular Tetravalent Cores. *J. Am. Chem. Soc.* **2015**, *137*, 8184–8191. [[CrossRef](#)] [[PubMed](#)]
19. Hao, Y.; Li, Y.; Song, L.; Deng, Z. Flash Synthesis of Spherical Nucleic Acids with Record DNA Density. *J. Am. Chem. Soc.* **2021**, *143*, 3065–3069. [[CrossRef](#)] [[PubMed](#)]
20. Melamed, J.R.; Kreuzberger, N.L.; Goyal, R.; Day, E.S. Spherical nucleic acid architecture can improve the efficacy of polycation-mediated siRNA delivery. *Mol. Ther. Nucleic Acids* **2018**, *12*, 207–219. [[CrossRef](#)]
21. Rische, C.H.; Goel, A.; Radovic-Moreno, A.F.; Gryaznov, S.M. Antibacterial silver core spherical nucleic acids. *Mater. Today Commun.* **2016**, *9*, 30–40. [[CrossRef](#)]
22. Zhang, C.; Hao, L.; Calabrese, C.M.; Zhou, Y.; Choi, C.H.J.; Xing, H.; Mirkin, C.A. Biodegradable DNA-Brush Block Copolymer Spherical Nucleic Acids Enable Transfection Agent-Free Intracellular Gene Regulation. *Small* **2015**, *11*, 5360–5368. [[CrossRef](#)] [[PubMed](#)]
23. Sprangers, A.J.; Hao, L.; Banga, R.J.; Mirkin, C.A. Liposomal Spherical Nucleic Acids for Regulating Long Noncoding RNAs in the Nucleus. *Small* **2017**, *13*, 1602753. [[CrossRef](#)] [[PubMed](#)]
24. Callmann, C.E.; Kusmierz, C.D.; Dittmar, J.W.; Broger, L.; Mirkin, C.A. Impact of Liposomal Spherical Nucleic Acid Structure on Immunotherapeutic Function. *ACS Cent. Sci.* **2021**, *7*, 892–899. [[CrossRef](#)]
25. Krishnamoorthy, K.; Hoffmann, K.; Kewalramani, S.; Brodin, J.D.; Moreau, L.M.; Mirkin, C.A.; de la Cruz, M.O.; Bedzyk, M.J. Defining the Structure of a Protein–Spherical Nucleic Acid Conjugate and Its Counterionic Cloud. *ACS Cent. Sci.* **2018**, *4*, 378–386. [[CrossRef](#)] [[PubMed](#)]
26. Banga, R.J.; Chernyak, N.; Narayan, S.P.; Nguyen, S.T.; Mirkin, C.A. Liposomal spherical nucleic acids. *J. Am. Chem. Soc.* **2014**, *136*, 9866–9869. [[CrossRef](#)] [[PubMed](#)]
27. Dimitrov, E.; Toncheva-Moncheva, N.; Bakardzhiev, P.; Forys, A.; Doumanov, J.; Mladenova, K.; Petrova, S.; Trzebicka, B.; Rangelov, S. Nucleic Acid-Based Supramolecular Structures: Vesicular Spherical Nucleic Acids from a Non-Phospholipid Nucleolipid. *Nanoscale Adv.* **2022**, *in press*. [[CrossRef](#)]
28. Ferrer, J.R.; Sinegra, A.J.; Ivancic, D.; Yeap, X.Y.; Qiu, L.; Wang, J.-J.; Zhang, Z.J.; Wertheim, J.A.; Mirkin, C.A. Structure-Dependent Biodistribution of Liposomal Spherical Nucleic Acids. *ACS Nano* **2020**, *14*, 1682–1693. [[CrossRef](#)]
29. Pickens, C.J.; Johnson, S.N.; Pressnall, M.M.; Leon, M.A.; Berkland, C.J. Practical Considerations, Challenges, and Limitations of Bioconjugation via Azide–Alkyne Cycloaddition. *Bioconjug. Chem.* **2018**, *29*, 686–701. [[CrossRef](#)]
30. Kanan, M.W.; Rozenman, M.M.; Sakural, K.; Snyder, T.M.; Liu, D.R. Reaction discovery enabled by DNA-templated synthesis and in vitro selection. *Nature* **2004**, *431*, 545–549. [[CrossRef](#)]
31. Provencher, S.W. Inverse Problems in Polymer Characterization: Direct Analysis of Polydispersity with Photon Correlation Spectroscopy. *Macromol. Chem.* **1979**, *180*, 201–209. [[CrossRef](#)]

32. Mladenov, N.; Petrova, S.D.; Mladenova, K.; Bozhinova, D.; Moskova-Doumanova, V.; Topouzova-Hristova, T.; Videv, P.; Veleva, R.; Kostadinova, A.; Staneva, G.; et al. Miscibility of hBest1 and sphingomyelin in surface films—A prerequisite for interaction with membrane domains. *Colloids Surf. B Biointerfaces* **2020**, *189*, 110893. [[CrossRef](#)] [[PubMed](#)]
33. Solomantin, S.; Herschlag, D. Methods of Site-Specific Labeling of RNA with Fluorescent Dyes. In *Methods Enzymology Book Series. Biophysical, Chemical, and Functional Probes of RNA Structure, Interactions and Folding: Part B*; Herschlag, D., Ed.; Elsevier: San Diego, CA, USA, 2009; Volume 469, Chapter 3; pp. 47–68.
34. Rangelov, S.; Petrova, E.; Berlinova, I.; Tsvetanov, C. Synthesis and Polymerization of Novel Oxirane Bearing an Aliphatic Double Chain Moiety. *Polymer* **2001**, *42*, 4483–4491. [[CrossRef](#)]
35. Bakardzhiev, P.; Rangelov, S.; Trzebicka, B.; Momekova, D.; Lalev, G. Nanostructures by Self-Assembly of Polyglycidol-Derivatized Lipids. *RSC Adv.* **2014**, *4*, 37208–37219. [[CrossRef](#)]
36. Stoyanova, B.; Novakov, C.; Tsvetanov, C.; Rangelov, S. Synthesis and Aqueous Solution Properties of Block Copolyethers with Latent Chemical Functionality. *Macromol. Chem. Phys.* **2016**, *217*, 2380–2390. [[CrossRef](#)]
37. Hoyle, C.E.; Bowman, C.N. Thiol–Ene Click Chemistry. *Angew. Chem. Int. Ed.* **2010**, *49*, 1540–1573. [[CrossRef](#)] [[PubMed](#)]
38. Olmsted, J.; Kearns, D.R. Mechanism of ethidium bromide fluorescence enhancement on binding to nucleic acids. *Biochemistry* **1977**, *16*, 3647–3654. [[CrossRef](#)] [[PubMed](#)]
39. Shen, C.-H. Diagnostic Molecular Biology. In *Detection and Analysis of Nucleic Acids*; Shen, C.-H., Ed.; Academic Press: New York, NY, USA, 2019; Chapter 7; pp. 167–185.
40. Hristova, K.; Needham, D. Phase behavior of lipid/polymer-lipid mixture in aqueous medium. *Macromolecules* **1995**, *28*, 991–1002. [[CrossRef](#)]
41. Nagle, J.F.; Tristram-Nagle, S. Structure of lipid bilayers. *Biochim. Biophys. Acta* **2000**, *1469*, 159–195. [[CrossRef](#)]
42. Cutler, J.; Zheng, D.; Xu, X.; Giljohann, D.; Mirkin, C.A. Polyvalent Oligonucleotide Iron Oxide Nanoparticle “Click” Conjugates. *Nano Lett.* **2010**, *10*, 1477–1480. [[CrossRef](#)]
43. Kusmierz, C.D.; Bujold, K.E.; Callmann, C.E.; Mirkin, C.A. Defining the Design Parameters for In Vivo Enzyme Delivery through Protein Spherical Nucleic Acids. *ACS Cent. Sci.* **2020**, *6*, 815–822. [[CrossRef](#)]
44. Zhu, S.; Xing, H.; Gordiichuk, P.; Park, J.; Mirkin, C.A. PLGA Spherical Nucleic Acids. *Adv. Mater.* **2018**, *30*, 1707113. [[CrossRef](#)] [[PubMed](#)]
45. Calabrese, C.M.; Merkel, T.J.; Briley, W.E.; Randeria, P.S.; Narayan, S.P.; Rouge, J.L.; Walker, D.A.; Scott, A.W.; Mirkin, C.A. Biocompatible infinite-coordination-polymer nanoparticle-nucleic-acid conjugates for antisense gene regulation. *Angew. Chem. Int. Ed.* **2015**, *54*, 476–480. [[CrossRef](#)]
46. Hurst, S.J.; Lytton-Jean, A.K.R.; Mirkin, C.A. Maximizing DNA Loading on a Range of Gold Nanoparticle Sizes. *Anal. Chem.* **2006**, *78*, 8313–8318. [[CrossRef](#)] [[PubMed](#)]
47. Escorihuela, J.; Banuls, M.-J.; Puchades, R.; Maquieira, A. Development of Oligonucleotide Microarrays onto Si-Based Surfaces via Thioether Linkage Mediated by UV Irradiation. *Bioconjug. Chem.* **2012**, *23*, 2121–2128. [[CrossRef](#)]
48. Hill, H.D.; Millstone, J.E.; Banholzer, M.J.; Mirkin, C.A. The role radius of curvature plays in thiolated oligonucleotide loading on gold. *ACS Nano* **2009**, *3*, 418–424. [[CrossRef](#)] [[PubMed](#)]
49. Alexander, S. Adsorption of chain molecules with a polar head a scaling description. *J. Phys. France* **1977**, *38*, 983–987. [[CrossRef](#)]
50. De Gennes, P. Conformations of Polymers Attached to an Interface. *Macromolecules* **1980**, *13*, 1069–1075. [[CrossRef](#)]
51. Bagatolli, L.A. To See or Not to See: Lateral Organization of Biological Membranes and Fluorescence Microscopy. *Biochim. Biophys. Acta* **2006**, *1758*, 1451–1456. [[CrossRef](#)]
52. Basu, S.; Dasgupta, N.N. Spectrophotometric Investigation of DNA in the Ultraviolet. *Biochim. Biophys. Acta* **1967**, *145*, 391–397. [[CrossRef](#)]
53. Tankovskaia, S.A.; Kotb, O.M.; Dommès, O.A.; Paston, S.V. DNA Damage Induced by Gamma-Radiation Revealed from UV Absorption Spectroscopy. *J. Phys. Conf. Ser.* **2018**, *1038*, 012027. [[CrossRef](#)]
54. Flory, P.J. *Principles of Polymer Chemistry*; Cornell University Press: Ithaca, NY, USA, 1953.